UNIVERSITÄT
DUISBURG
ESSEN

Offen im Denken

Universität Duisburg-Essen
Institut für Mechanik
Fakultät für Ingenieurwissenschaften
Abteilung Bauwissenschaften
Prof. Dr.-Ing. J. Schröder

An Algorithmic Scheme for the Automated Calculation of Fiber Orientations in Arterial Walls

by S. Fausten, D. Balzani, & J. Schröder

type of report:
Preprint

submitted to
Computational Mechanics
on February 18, 2016

Report - Preprint	**No. 122**

04. März 2016

Editor: Prof. Dr.-Ing. habil. Jörg Schröder
Universitätsstraße 15, 45141 Essen, Germany

An Algorithmic Scheme for the Automated Calculation of Fiber Orientations in Arterial Walls

Simon Fausten[1], Daniel Balzani[2] and Jörg Schröder[1]

[1]Institut für Mechanik, Fachbereich für Ingenieurwissenschaften/Abtl. Bauwissenschaften
Universität Duisburg-Essen, 45141 Essen, Universitätsstr. 15, Germany
e-mail: j.schroeder@uni-due.de, phone: +49 201 183 2708, fax: +49 201 183 2680
e-mail: simon.fausten@uni-due.de, phone: +49 201 183 2679, fax: +49 201 183 2680

[2]Institut für Mechanik und Flächentragwerke/Fakultät Bauingenieurwesen
TU Dresden, 01187 Dresden, Nürnberger Straße 31A, Germany
and Dresden Center for Computational Materials Science (DCMS), 01062 Dresden
e-mail: daniel.balzani@tu-dresden.de, phone: +49 351 463 4 32 31, fax: +49 351 463 4 32 35

Abstract

We propose an algorithmic scheme for the numerical calculation of fiber orientations in arterial walls. The basic assumption behind the procedure is that the fiber orientations are mainly governed by the principal tensile stress directions resulting in an improved load transfer within the artery as a consequence of the redistribution of stresses. This reflects the biological motivation that soft tissues continuously adapt to their mechanical environment in order to optimize the load-bearing capacities. The algorithmic scheme proposed here enhances efficiency of the general procedure given in Hariton et al. [2007a], which consists of repeatedly identifying a favored fiber orientation based on the principal tensile stresses under a certain loading scenario, and then re-calculating the stresses for that loading scenario with the modified favored fiber orientation. Since the method still depends on a highly accurate stress approximation of the finite element formulation, which is not straightforward to obtain in particular for incompressible and highly anisotropic materials, furthermore, a modified model is introduced. This model defines the favored fiber orientation not only in terms of the local principal stresses, but in terms of the volume averages of the principal stresses computed over individual finite elements. Thereby, the influence of imperfect stress approximations can be weakened leading to a stabilized convergence of the reorientation procedure and a more reasonable fiber orientation with less numerical noise. The performance of the proposed fiber reorientation scheme is investigated with respect to different finite element formulations and different favored fiber orientation models, Hariton et al. [2007a] and Cyron and Humphrey [2014]. In addition to that, it is applied to calculate the fiber orientation in a patient-specific arterial geometry.

Keywords: Fiber Reorientation, Collagen Fibers, Arterial Walls, Finite Element Method

1. Introduction

The collagen fibers in arterial tissues and their orientation are of major importance for the overall mechanical behavior of arterial walls, i.e. the description of the passive response and transmural stress distribution of the arterial tissue. In computational biomechanics soft biological tissues are usually described by quasi-incompressible highly nonlinear anisotropic material models, e.g. Holzapfel et al. [2000] and Balzani et al. [2006]. Multilayered fiber-reinforced materials which are characterized by two main fiber families

embedded in a soft matrix material turned out to be a suitable choice for the material description. The fibers are arranged crosswise helically around the artery in axial direction. However, the in-vivo identification of patient-specific fiber orientations in real arteries, whose geometry significantly differs from an idealized thick-walled tube, in particular for atherosclerotic arteries, is difficult. There, strong curvatures and irregular non-rotationally symmetric cross-sections may be observed. Therefore, numerical methods enabling an automated calculation of fiber orientations based on biologically motivated assumptions regarding favored orientations present a suitable framework. This strategy is in line with the living nature of biological tissues, which continuously change and adapt according to their mechano-biological environment in order to improve the load-bearing capacities. The consideration of such biomechanically motivated fiber reorientation approaches may yield a more realistic description of arterial tissues with distributed orientations through the thickness of the vessel wall (O'Connell et al. [2008] and Schriefl et al. [2012]), which goes beyond the assumption of a constant fiber orientation in each layer of the tissue.

In the literature the reorientation of collagen fibers is usually motivated by either stress or stretch. In Driessen et al. [2004] the well-known material model from Holzapfel et al. [2000] is combined with a mathematical model, aligning the fiber orientations with the principal stretch directions. This approach is extended in Driessen et al. [2008] towards specific stimulus functions for the fiber remodeling, considering strain- as well as stress-based arguments for the remodeling of collagen fibers in arterial walls and aortic heart valves. A stress-driven model is proposed in Hariton et al. [2007a], where the orientation of the collagen fibers is determined by the direction and magnitude of the principal stresses. This model is applied to the special case of a human carotid bifurcation in Hariton et al. [2007b]. A completely different approach, which is also stress-driven, is given in Kuhl and Holzapfel [2007] and is based on the remodeling of orthotropic unit cells, motivated by phenomenologically based micro-structural considerations on the collagen fiber level. Another approach based on a micro-mechanically motivated formulation, taking into account a unit sphere with the unit vectors as internal variables is proposed in Menzel and Waffenschmidt [2009]. In Himpel et al. [2008] the time-dependent fiber reorientation of transversely isotropic continua and its algorithmic implementation based on principal stretches is discussed. In order to consider realistic collagen fiber orientations in patient-specific arteries, taking into account a strain-based remodeling algorithm, a remodeling metric is introduced in Creane et al. [2012], which is an extension of Creane et al. [2011]. Besides the stress- and stretch-driven models several other approaches towards fiber reorientation can be found. Grillo et al. [2015] for example present a mathematical model for the structural reorganization of fibers based on the principle of virtual power and dissipation, applicable to fiber-reinforced composites as well as soft biological tissues. Another interesting theoretical approach is found in Cyron and Humphrey [2014], where findings from the netting analysis are applied to membrane theory. In Waffenschmidt and Menzel [2014] energy arguments are taken into account to determine the fiber orientations. A recent publication by Qi et al. [2015] compares different fiber reorientation approaches and their applicability to the special case of the human iliac arteries. However, in order to obtain a robust numerical scheme enabling the computation of the fiber orientation only requiring a minimum of patient-specific parameters, a simple method is necessary and thus, the general procedure in Hariton et al. [2007a] appears to be advantageous. Hence, we extend this approach such that two main advantages are obtained: a higher efficiency in terms of less reorientation iterations and a stabilized model based on the principal

stresses of the volumetric average of the Cauchy stresses tensor computed over each finite element. By detailed numerical analysis comparing different finite element formulations and favored fiber orientation models we show that this stabilized model enables an improved convergence of the reorientation algorithm as well as a more reasonable distribution of fiber orientation with less numerical noise.

The remaining paper is organized as follows: the continuum mechanical material model for the vessel wall is briefly recapitulated in Section 2. In the following Section 3 the stress-driven reorientation approach is described as well as the implementation of the approach with respect to the underlying algorithm. Various numerical results for the simulation of fiber reorientation in arterial walls, considering several finite element formulations and different boundary value problems, are presented in Section 5. Finally the paper closes with a conclusion in Section 6.

2. Continuum Mechanical Description of Arterial Tissues

Let $\boldsymbol{\varphi}$ denote the non-linear deformation, which maps points $\boldsymbol{X}$ of the reference configuration $\mathcal{B}_0$ onto points $\boldsymbol{x}$ of the actual configuration $\mathcal{B}_t$. The deformation gradient, defined by $\boldsymbol{F} = \mathrm{Grad}\,\boldsymbol{\varphi}$ and the right Cauchy-Green tensor $\boldsymbol{C} = \boldsymbol{F}^T\boldsymbol{F}$, are introduced as deformation measures. The anisotropic material behavior of arterial tissues results mainly from the reinforcing collagen fibers. They are considered to be mainly arranged in two fiber directions cross-wise helically around the arterial wall. In order to describe the orientations of the collagen fiber bundles we use the concept of structural tensors, see e.g. Boehler [1987]. Hence, an additively decoupled strain energy ψ consisting of an isotropic part ψ^{isot} for the elastin-rich ground substance and the superposition of two transversely isotropic parts $\psi^{\mathrm{ti}}_{(a)}$ for each of the individual fiber families $a = 1, 2$ is postulated. The fiber orientations are characterized by the unit vectors $\boldsymbol{A}_{(a)}$ describing the preferred directions in the reference configuration. Furthermore, it is assumed that only a weak interaction between the two fiber families exists. In order to fulfill the objectivity condition a priori, the isotropic energy is considered to depend on the right Cauchy-Green tensor, i.e., $\psi := \psi(\boldsymbol{C})$. For the transversely isotropic part the structural tensor $\boldsymbol{M}_{(a)} = \boldsymbol{A}_{(a)} \otimes \boldsymbol{A}_{(a)}$ for $a = 1, 2$, acts as an additional argument tensor such that the strain energy reads $\psi^{\mathrm{ti}}_{(a)} := \psi^{\mathrm{ti}}_{(a)}(\boldsymbol{C}, \boldsymbol{M}_{(a)})$. A convenient representation of the strain energy function can be obtained considering the principal and mixed invariants

$$I_1 = \mathrm{tr}\boldsymbol{C}\,,\; I_2 = \mathrm{tr}[\mathrm{Cof}\boldsymbol{C}]\,,\; I_3 = \det\boldsymbol{C}\,,\; K_3^{(a)} = \mathrm{tr}[\mathrm{Cof}\boldsymbol{C}(\boldsymbol{1} - \boldsymbol{M}_{(a)})], \tag{1}$$

where $\mathrm{Cof}\boldsymbol{C} = \det[\boldsymbol{C}]\boldsymbol{C}^{-T}$ denotes the cofactor of $\boldsymbol{C}$. It should be noted that the invariants in (1) are polyconvex in the sense of Ball [1977], see Schröder and Neff [2003] and Schröder [2010]. Finally, the strain energy function for two fiber families reads

$$\psi(\boldsymbol{C}, \boldsymbol{M}_{(1)}, \boldsymbol{M}_{(2)}) = \psi^{\mathrm{isot}}(I_1, I_3) + \sum_{a=1}^{2} \psi^{\mathrm{ti}}_{(a)}(I_1, K_3^{(a)}). \tag{2}$$

Here, polyconvex energy functions are considered, since this condition with an additional coercivity condition is essential to ensure the existence of minimizers and material stability. For a detailed analysis of material stability in the framework of anisotropic hyperelasticity see Schröder et al. [2005]. In detail a Neo-Hooke-type function is considered for the

isotropic part and for the transversely isotropic part the function for arterial tissues proposed in Balzani et al. [2006] is used. The latter has been successfully applied in massive parallel calculations of patient-specific atherosclerotic arteries, see Balzani et al. [2012]. The complete strain energy function is given by

$$\psi^{\text{isot}} = \epsilon_1 \left(I_3^{\epsilon_2} + I_3^{-\epsilon_2} - 2 \right) + c_1 \left(I_1 \, I_3^{-1/3} - 3 \right) \quad \text{and} \quad \psi^{ti}_{(a)} = \alpha_1 \left\langle K_3^{(a)} - 2 \right\rangle^{\alpha_2}, \tag{3}$$

where the restrictions $c_1 > 0, \epsilon_1 > 0, \epsilon_2 > 1, \alpha_1 > 0$ and $\alpha_2 > 2$ ensure polyconvexity and smooth tangent moduli; and the Macaulay brackets are defined as $\langle(\bullet)\rangle = 1/2(|(\bullet)| + (\bullet))$. It is important to note that a volumetric-isochoric split is only considered for the isotropic part of the function, while it is not considered for the transversely isotropic part, in this context we refer to the discussion in Sansour [2008]. The second Piola-Kirchhoff stresses and the Cauchy Stresses are computed by $\boldsymbol{S} = 2\partial_{\boldsymbol{C}}\psi(\boldsymbol{C})$ and $\boldsymbol{\sigma} = (\det[\boldsymbol{F}])^{-1}\boldsymbol{F}\boldsymbol{S}\boldsymbol{F}^T$, respectively. Various polyconvex isotropic volumetric functions are given in Hartmann and Neff [2003].

3. Numerical Approach for Fiber Reorientation

Following the approach in Hariton et al. [2007a], the algorithm conceptionally consists of two parts, which are repeatedly considered in each *reorientation step* until a converged fiber orientation is obtained. These two parts are (i) calculation of a favored fiber orientation based on the principle stresses, which are computed for a specific load-scenario, and (ii) accommodation of equilibrium for the same load-scenario with the modified favored fiber orientation. In the original algorithm, the equilibrium conditions are computed by fixating the modified fiber orientation and step-wise increasing the load by applying a specified number of load steps $n_{(\text{HDGH})}$, where in each incremental load step the boundary value problem is solved using a Newton iteration. In our algorithm the way differs how equilibrium is accommodated for each reorientation step. We do not fixate the fiber orientation, but consider a number $n_{(\text{FBS})}$ of incremental updates of fiber orientation until the favored fiber orientation is achieved. In each of these incremental reorientation steps, we also solve the associated boundary value problem using a Newton iteration. Since in each of the incremental steps, either incremental load or incremental reorientation step, a comparable number of Newton iterations is required to solve the boundary value problem, the main improvement in efficiency is realized if $n_{(\text{FBS})} < n_{(\text{HDGH})}$. For most problems this behavior is expected. In particular for difficult numerical problems, e.g. if the fluid-structure interaction of the vessel wall with the blood flow is taken into account, the required number of incremental load steps easily reaches $n_{(\text{HDGH})} > 1000$ (cf. Balzani et al. [2015]) and will be rather constant over all reorientation steps, no matter how strong the favored fiber orientation changes in each reorientation step. In our approach the number of incremental reorientation steps is rather independent on the complexity of the numerical problem. Furthermore, it typically reduces during the reorientation scheme since the required change in favored fiber orientation also reduces resulting in less incremental steps. In addition to that, for the fiber orientation scheme a reasonable experience-based initial fiber orientation may be available, even reducing the required number of incremental reorientation steps further. This experience-based initial configuration, reducing the required number of load steps, typically lacks availability. In order to measure the gain in efficiency of our

approach, an efficiency factor f_{comp} may be defined as

$$f_{\text{comp}} := \frac{n^{\text{total}}_{(\text{FBS})}}{n^{\text{total}}_{(\text{HDGH})}} \,. \tag{4}$$

Herein, $n^{\text{total}}_{(\text{HDGH})}$ and $n^{\text{total}}_{(\text{FBS})}$ denote the total number over all reorientation steps of incremental load steps (approach of Hariton et al. [2007a]) and incremental orientation steps (our approach) until a converging fiber orientation is obtained. Thus, a number of $f_{\text{comp}} = 0.5$ means that our approach requires half of the calculations of equilibrium and thus approximately half as much computing time until a converging fiber orientation is obtained. For identical definitions of favored fiber orientations the number of reorientation steps will be the same for both approaches, it is the number of incremental steps in each reorientation step which differs.
Note that in the proposed approach the direct incorporation of history-dependency, either in terms of dissipative materials or inertia during the diastolic-systolic blood pressure cycle, will lead to different results compared with the approach in Hariton et al. [2007a]. This is due to the fact that here we do not re-compute the full load-path for the modified favored fiber orientation in each reorientation step. Therefore, an extended termination criterion may be required based on such full load-path calculations to ensure that also for the history-dependent behavior a converged state is obtained. For most arterial wall simulations, however, the material behavior is assumed to be hyperelastic and then the presented approach can be applied without any restriction.

3.1. Stress-Driven Reorientation Model based on Local Stresses σ^l

For any kind of fiber orientation calculation a model is required for the determination of the favored fiber orientation. Similar to the approach described by Hariton et al. [2007a] the approach considered here is based on the assumption that the fiber orientation is mainly driven by the principal tensile stress directions, in order to improve the load-bearing capacities of the tissue. Since mainly two fiber families exist, their favored orientation may be determined by the directions of the first two principal stresses. Therefore, in each material point the numerical solution of the eigenvalue problems $(\boldsymbol{\sigma} - \sigma \mathbf{1}) \cdot \hat{\boldsymbol{e}} = \underline{0}$ with the characteristic polynomial $\det(\boldsymbol{\sigma} - \sigma \mathbf{1})$ is considered and yields the principal stresses $\sigma_I \geq \sigma_{II} \geq \sigma_{III}$ and principal directions $\hat{\boldsymbol{e}}_I, \hat{\boldsymbol{e}}_{II}$ and $\hat{\boldsymbol{e}}_{III}$ of the Cauchy stress tensor $\boldsymbol{\sigma}$. The stress tensor with respect to its principal axes is then given by

$$\boldsymbol{\sigma} = \sum_{i=I,II,III} \sigma_i \hat{\boldsymbol{e}}_i \otimes \hat{\boldsymbol{e}}_i. \tag{5}$$

It is assumed that the biological fiber directions are located in the plane spanned by the eigenvectors associated to the two largest tensile principal stresses, while maintaining symmetry to each other with respect to the eigenvector associated to the largest tensile principal stress $\hat{\boldsymbol{e}}_I$. Hence, the favored fiber orientation in the actual configuration can beexpressed as

$$\begin{aligned} \boldsymbol{a}_{(1)} &= \langle \sigma_I \rangle \hat{\boldsymbol{e}}_I + \langle \sigma_{II} \rangle \hat{\boldsymbol{e}}_{II} \\ \boldsymbol{a}_{(2)} &= \langle \sigma_I \rangle \hat{\boldsymbol{e}}_I - \langle \sigma_{II} \rangle \hat{\boldsymbol{e}}_{II}. \end{aligned} \tag{6}$$

The Macaulay brackets ensure that only tensile principal stresses are taken into account for the reorientation. In addition to that, this formulation also covers the special case that only

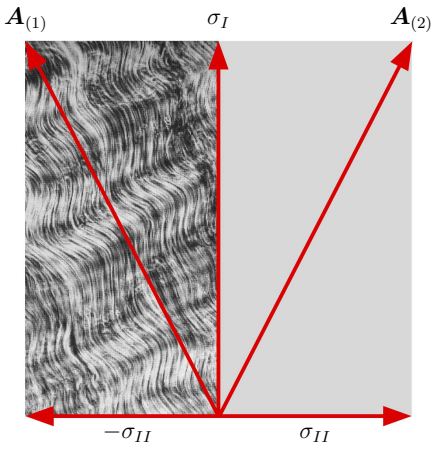

Figure 1: Schematic illustration of the optimal fiber orientation with respect to the principal stresses and their associated directions.

one and not two tensile principal stresses occur in a material point. In this case both fiber families reorient in the direction of the remaining tensile principal stress. The geometric interpretation of (6) is illustrated in Figure 1. Since, the material model is formulated in the reference configuration it is necessary to pull-back the orientation vectorsby

$$\boldsymbol{A}_{(1)} = \frac{\boldsymbol{F}^{-1}\boldsymbol{a}_{(1)}}{|\boldsymbol{F}^{-1}\boldsymbol{a}_{(1)}|}, \quad \boldsymbol{A}_{(2)} = \frac{\boldsymbol{F}^{-1}\boldsymbol{a}_{(2)}}{|\boldsymbol{F}^{-1}\boldsymbol{a}_{(2)}|}. \tag{7}$$

3.2. Stress-Driven Reorientation Model based on Element Averages $\bar{\sigma}$

The stress-driven reorientation procedure apparently depends strongly on the quality of the stress approximation in the numerical scheme used for the spatial discretization. Therefore, depending on the particular finite element formulation, numerically scattered stresses may lead to a non-converging reorientation scheme. In order to reduce the sensitivity with respect to such local scattering and to improve the stability of the method, in this section an extended model is presented. Here, the stress distribution is smoothed by calculating volume averaged stress quantities over the associated finite element $\mathcal{B}^e$. Therefore, the averaged stress $\bar{\boldsymbol{\sigma}}$ is introduced based on the Cauchy Stresses as

$$\bar{\boldsymbol{\sigma}} = \frac{1}{v^e} \int_{\mathcal{B}_t^e} \boldsymbol{\sigma} \mathrm{d}v, \text{ with } v^e = \int_{\mathcal{B}_t^e} \mathrm{d}v. \tag{8}$$

Herein, $\mathrm{d}v$ denotes an infinitesimal volume element in the actual configuration. Based on this quantity the local principal stresses $\bar{\sigma}_I$, $\bar{\sigma}_{II}$ and $\bar{\sigma}_{III}$ as well as the associated principal directions are calculated. The biological orientation of the fibers in the actual configuration is then assumed as

$$\begin{aligned} \boldsymbol{a}_{(1)} &= \langle \bar{\sigma}_I \rangle \hat{\boldsymbol{e}}_I + \langle \bar{\sigma}_{II} \rangle \hat{\boldsymbol{e}}_{II} \\ \boldsymbol{a}_{(2)} &= \langle \bar{\sigma}_I \rangle \hat{\boldsymbol{e}}_I - \langle \bar{\sigma}_{II} \rangle \hat{\boldsymbol{e}}_{II}. \end{aligned} \tag{9}$$

The pull-back of the fiber orientation into the reference configuration is done analogously to equation (7) with the deformation gradient $\boldsymbol{F}$.

3.3. Algorithm for the Incremental Fiber Update

For the implementation of the above described reorientation models an iterative algorithm, based on incremental fiber orientation updates, is proposed. Instead of recomputing the complete BVP with an updated fiber orientation, cf. Hariton et al. [2007a], here the fiber orientation is changed directly in the deformed configuration. A change of the fiber orientation will require a repeated computation of the solution; obviously large changes of the fiber orientation could lead to convergence problems in the Newton-Iteration. Therefore, only incremental updates of the fiber orientation are taken into account. First of all the target difference vector

$$\Delta \boldsymbol{A}_{(a)}^{k} = \boldsymbol{A}_{(a)}^{k} - \boldsymbol{A}_{(a)}^{k-1}, \tag{10}$$

is defined as the difference between the actual fiber orientation $\boldsymbol{A}_{(a)}^{k-1}$ and the favored target orientation vectors $\boldsymbol{A}_{(a)}^{k}$. The initial value $\boldsymbol{A}_{(a)}^{0}$ denotes the orientation at the beginning of the fiber update scheme and k denotes the actual reorientation step. Furthermore the enclosedangle

$$\measuredangle(\boldsymbol{A}_{(a)}^{k}, \boldsymbol{A}_{(a)}^{k-1}) = \beta^{k} \tag{11}$$

is computed. Instead of applying the complete difference vector only increments of the target difference vector $\phi^{j}\Delta\boldsymbol{A}_{(a)}^{k,j}$ with $\phi^{j} \in [0,1]$ are added in separated steps, such that the incremental update of the fiber orientation yields

$$\boldsymbol{A}_{(a)}^{k,j} := \frac{\boldsymbol{A}_{(a)}^{k,j-1} + \phi^{j}\Delta\boldsymbol{A}_{(a)}^{k,j}}{|\boldsymbol{A}_{(a)}^{k,j-1} + \phi^{j}\Delta\boldsymbol{A}_{(a)}^{k,j}|} \quad \text{with} \quad \Delta\boldsymbol{A}_{(a)}^{k,j} = \boldsymbol{A}_{(a)}^{k} - \boldsymbol{A}_{(a)}^{k,j-1}, \tag{12}$$

with j denoting the incremental reorientation step and ϕ^{j} denoting a scalar-valued factor which is chosen such that

$$\beta^{k,j} := \measuredangle(\boldsymbol{A}_{(a)}^{k,j}, \boldsymbol{A}_{(a)}^{k,j-1}) \leq \beta_{\max}, \tag{13}$$

is fulfilled with the user-defined maximum reorientation angle $\beta_{\max}$. Here, $\boldsymbol{A}_{(a)}^{k,0}$ is initialized by $\boldsymbol{A}_{(a)}^{k-1}$ and serves as starting point for the incremental updates in respective reorientation steps. A schematic illustration of the incremental fiber orientation update is given in Figure 2. The incremental update algorithm is repeated until the target fiber orientation in each Gaußpoint (GP) of the considered BVP is obtained. After each complete incremental reorientation loop, i.e. when the target fiber orientation $\boldsymbol{A}_{(a)}^{k}$ is reached, a new stress state results from accommodating equilibrium for a modified fiber orientation field. Therefore, a new favored target fiber orientation is computed at each GP in the next reorientation step. This iterative process is continued until the change of the fiber orientation between two reorientation steps is within a specified tolerance, i.e. when the norm of the total difference vector falls below a certain tolerance $\Delta\boldsymbol{A}_{(a)}^{k} < tol$ in all Gaußpoints of the considered BVP. A detailed description of the complete reorientation process, including the nested incremental reorientation loop is presented in the algorithmic box inTable 1.

4 Comparison with the Model of Cyron and Humphrey [2014]

Another interesting model for a biologically favored fiber reorientation based on theoretical considerations is found in Cyron and Humphrey [2014]. There, the arterial wall is

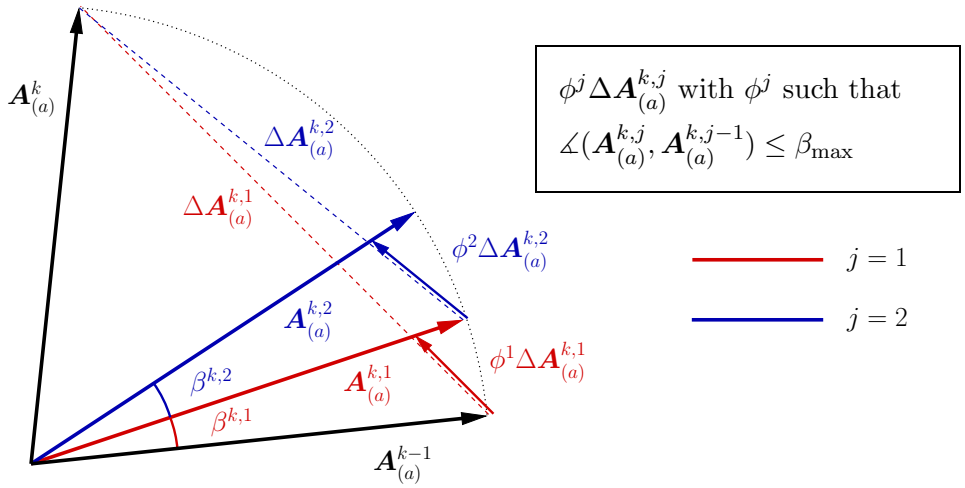

Figure 2: Schematic illustration of the fiber update: Initial value $\boldsymbol{A}^{k-1}_{(a)}$, including the incremental updates $\boldsymbol{A}^{k,j}_{(a)}$ based on the incremental differences $\Delta\boldsymbol{A}^{k,j}_{(a)}$ and the favored target fiber orientation $\boldsymbol{A}^{k}_{(a)}$ in the reorientation step k.

Table 1: Algorithmic box for the computation of final favored fiber orientations.

(1) Prescribe suitable initial fiber orientation $\boldsymbol{A}^{0}_{(a)}$

(2) Solve the BVP $\rightarrow$ $\{\boldsymbol{u}, \boldsymbol{C}, \boldsymbol{\sigma}\}$

(3) Reorientation loop for adapting favored fiber orientation (over k):

(3.1) Calculate principal stresses $\sigma_I, \sigma_{II}, \sigma_{III}$

(3.2) Compute target orientation vectors $\boldsymbol{A}^{k}_{(a)}$

(3.3) Target total difference vector $\Delta\boldsymbol{A}^{k}_{(a)} = \boldsymbol{A}^{k}_{(a)} - \boldsymbol{A}^{k-1}_{(a)}$

(3.4) If $|\Delta\boldsymbol{A}^{k}_{(a)}| < tol$ in all GPs

$\rightarrow$ final fiber orientation obtained, exit loop

(3.5) Incremental reorientation loop over j:

(3.5.1) Incremental update of fiber orientation

$$\boldsymbol{A}^{k,j}_{(a)} := \frac{\boldsymbol{A}^{k,j-1}_{(a)} + \phi^j\Delta\boldsymbol{A}^{k,j}_{(a)}}{|\boldsymbol{A}^{k,j-1}_{(a)} + \phi^j\Delta\boldsymbol{A}^{k,j}_{(a)}|}$$

with $\Delta\boldsymbol{A}^{k,j}_{(a)} = \boldsymbol{A}^{k}_{(a)} - \boldsymbol{A}^{k,j-1}_{(a)}$, see also Eq.(13)

(3.5.2) Solve the actual BVP with updated orientations

(3.5.3) $|\boldsymbol{A}^{k,j}_{(a)} - \boldsymbol{A}^{k}_{(a)}| = 0$ in all GPs $\rightarrow$ exit loop for next adaption of fiber orientation (updated stress scenario)

described by a perfect tube composed of multiple stacked membranes and the fiber orientation in each membrane is influenced by the pulse pressure, the wall thickness and the

resulting Cauchy *membrane* stresses T_{11} and T_{22} in circumferential and axial direction. Two symmetric fiber families aligned in the directions $\pm\bar{\theta}$ are considered, where $\bar{\theta}$ measures the angle relative to the circumferential direction. According to the model of Cyron and Humphrey [2014] the fiber orientations are considered to be

$$\bar{\theta} = \arctan\sqrt{T_{22}/T_{11}}. \tag{14}$$

In order to compare this model with the models considered in this paper we replace the membrane stresses by the first and second principal Cauchy stress

$$\bar{\theta} = \arctan\sqrt{T_{22}/T_{11}} \approx \arctan\sqrt{\sigma_{II}/\sigma_I} \tag{15}$$

and define $\bar{\theta}$ to be the angle with respect to the direction of the first principal stress. Indeed, for a perfect tube as it is used in Cyron and Humphrey [2014] the circumferential and axial membrane stresses align with the principal membrane stresses. Thus, the fiber directions are obtained based on the angle $\bar{\theta}$ by

$$\boldsymbol{a}_{(1)} = \cos\bar{\theta}\ \boldsymbol{e}_I + \sin\bar{\theta}\ \boldsymbol{e}_{II} \quad \text{and} \quad \boldsymbol{a}_{(2)} = \cos\bar{\theta}\ \boldsymbol{e}_I - \sin\bar{\theta}\ \boldsymbol{e}_{II}. \tag{16}$$

Now both models are compared in a series of biaxial tension tests, where the new algorithmic scheme from Section 3.3 is applied. We align the x_1- and x_2-coordinate axis in the biaxial tensile axis and set

$$\sigma_{11} = \sigma_0 \quad \text{and} \quad \sigma_{22} = \lambda\sigma_0 \quad \text{with} \quad \sigma_0 = 10 \text{ kPa},\ \lambda \in [0, 1). \tag{17}$$

The results are depicted in Figure 3, where the resulting fiber angle $\bar{\theta}$, the according total energy ψ, its isotropic part ψ_{iso} and its transversely isotropic part ψ_{ti} are compared. Here, it is observed that the total energy is higher on the whole interval of λ for the approach of Cyron and Humphrey [2014] compared to the model of Hariton et al. [2007a]. Interestingly, the transversely isotropic part of the energy is lower in the interval $\lambda = [0.4, 0.8]$. Nevertheless, the isotropic part as well as the total energy are still higher for the model of Cyron and Humphrey [2014]. Hypothesizing that a biologically motivated approach would favor an energy-minimizing model we focus on the models explained in Sections 3.1 and 3.2 in subsequent investigations.

5. Numerical Examples

In this section several numerical examples, illustrating the different approaches for the fiber reorientation, are presented. In all examples the arterial tissue is modeled with the strain energy function known from Balzani et al. [2006]. We use the set of material parameters from Brands et al. [2008], which has been fitted to experimental data of human arterial tissue from Holzapfel [2006]. The material parameters are listed in Table 2. All presented simulations were done with the multi-purpose finite element analysis program FEAP8.2, see Taylor [2014].

5.1. Uniaxial Displacement

The first numerical example is a uniaxial unconstrained tension test. Here, a stretch of 3% of the original length is applied in x_1-direction and the fiber directions are recomputed in

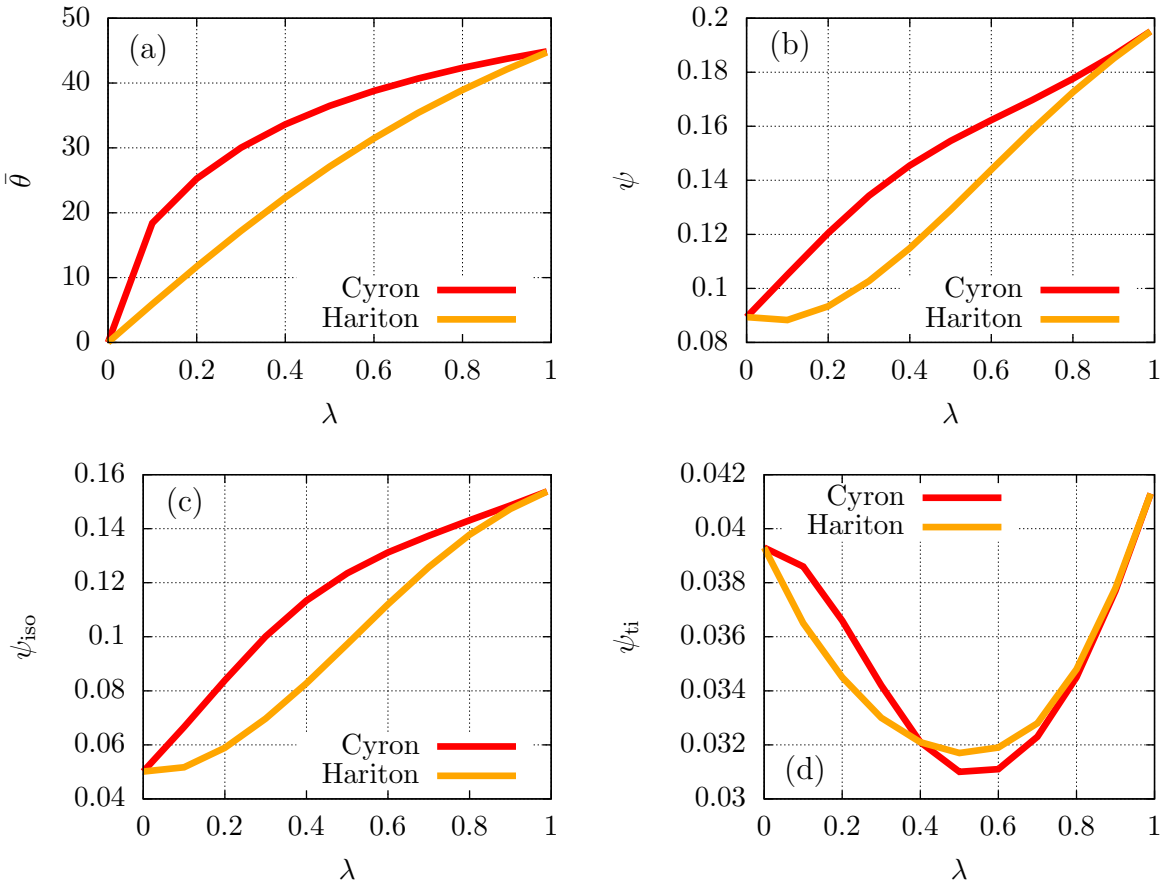

Figure 3: Biaxial-tension test for the models of Cyron and Humphrey [2014] and Hariton et al. [2007a]: (a) fiber angle $\bar{\theta}$, (b) strain energy ψ, (c) isotropic strain energy ψ_{iso} and (d) transversely isotropic strain energy ψ_{ti}.

Layer	c_1 kPa	ϵ_1 kPa	ϵ_2 -	α_1 kPa	α_2 -
media	17.5	499.8	2.4	30001.9	5.1

Table 2: Parameters for human media (Brands et al. [2008]).

the deformed configuration. In this academic example the solution is known a priori and therefore it is used to illustrate the proposed stress-driven update scheme and show its feasibility. The BVP, illustrated in Figure 4, is discretized by tetrahedral elements. Note that since a homogeneous BVP is considered, the FE formulation as well as the number of elements does not matter, and thus, the FE method is only used to adjust the zero stress conditions related with the uniaxial tension conditions. A fiber orientation exclusively located in the $x_1 - x_2$ plane and a fiber angle of $\beta_f = 30°$ with respect to the x_1-direction is considered as initial configuration. As expected the fibers reorient in the direction of the largest principal stress, i.e. in x_1-direction.

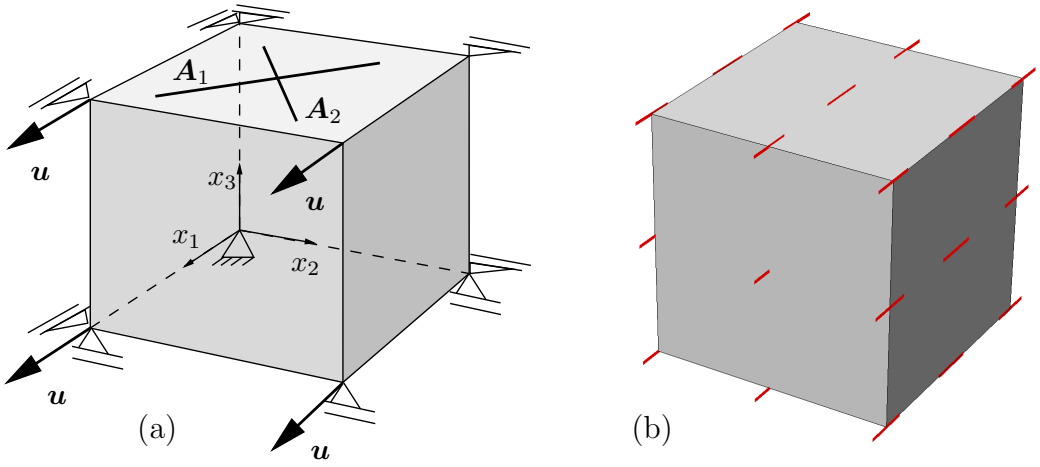

Figure 4: (a) BVP for uniaxial unconstrained tension with two preferred fiber directions (b) fiber orientations obtained after the reorientation process.

5.2. Idealized Arterial Geometry

The second numerical example considers a simple idealized arterial geometry, i.e. a thick-walled tube with an inner radius of 4.0 mm and thickness of 2.5 mm, composed of only the media layer. Furthermore, symmetry boundary conditions are applied such that only a quarter of the tube with an height of 1.0 mm is taken into account. An internal blood pressure of 10 kPa is applied onto the inner surface and while the displacement at the top and bottom plane is constrained in axial direction, the geometry is allowed to extend freely in radial direction, cf. Figure 5(a).

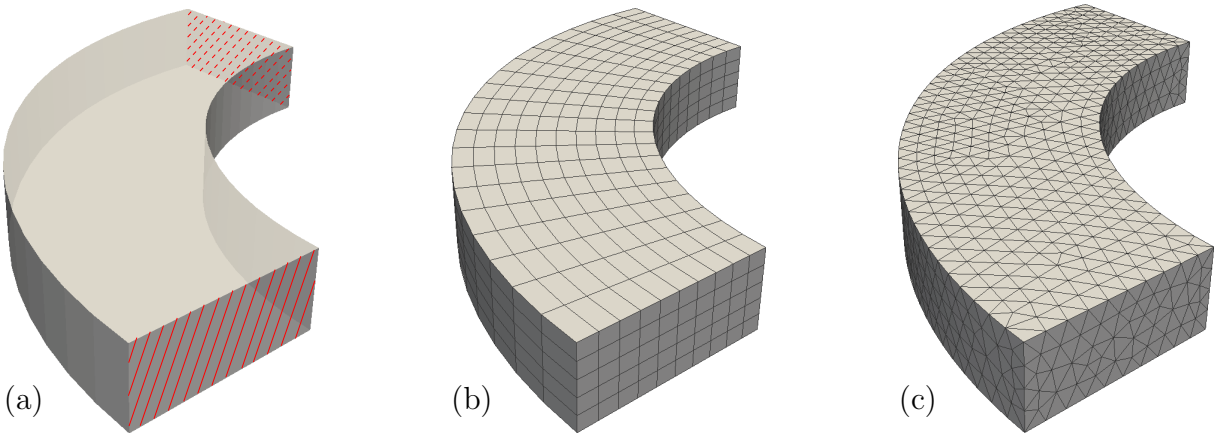

Figure 5: (a) Idealized arterial geometry including Dirichlet boundary conditions, shaded areas are constrained in circumferential direction. (b) Mesh using 1000 P_2-Brick-Elements with 28.413 degrees of freedom and (c) Mesh using 8385 P_2-Tetrahedral-Elements with 40.731 degrees of freedom.

The initial fiber orientation is given by a fiber angle of 30° with respect to the circumferential direction and the fibers are winding cross-wise helically around the arterial wall. With the help of this simple but reasonable BVP different finite element formulations and different reorientation approaches are compared. The finite element meshes are depicted in Figure 5(b) and (c). In total five different settings analyzing the approach based on local stresses σ^l as well as averaged stresses $\bar{\sigma}$ are compared:

- Approach σ^l with P_2 brick elements, 20 noded
- Approach σ^l with P_2 tetrahedral elements, 10 noded
- Approach σ^l with tetrahedral $\bar{F}$-elements, 10 noded
- Approach $\bar{\sigma}$ with P_2 tetrahedral elements, 10 noded
- Approach $\bar{\sigma}$ with tetrahedral $\bar{F}$-elements, 10 noded

The $\bar{F}$-elements take into account a mixed formulation with discontinuous element-wise constant approximation of the volume dilatation and quadratic interpolation of the displacements, cf. Simo et al. [1985]. We investigate different finite element formulations because apparently, the reorientation procedure strongly depends on the quality of the stress approximations. The resulting convergence behavior and the resulting fiber angle distribution, evaluated for the individual Gauss-points, are depicted in Figure 6. For all computations a maximal reorientation angle of $\beta_{\max} = 5^\circ$ and a stopping criterion of $tol = 0.0175$ is considered.

Approach σ^l with P_2 brick elements: For reorientation approach σ^l the resulting fiber orientation as well as the reorientation behavior are depicted in Figure 6(a). A final fiber orientation is achieved within $n^{\text{total}}_{(\text{FBS})} = 15$ incremental reorientation steps, i.e. 5 reorientation steps and 44 Newton iterations, where each reorientation step is identified as one peak in the graph shown in Figure 6(a). The result is a smooth fiber distribution over the radius ranging between 1° and 25°, which is qualitatively in good agreement with the results presented in Hariton et al. [2007a]. Such distributed fiber orientations have also been experimentally observed. In O'Connell et al. [2008] measurements, using 3D confocal and electron microscopy imaging on healthy rat abdominal aorta of collagen and SMC (Smooth Muscle Cell) nuclei, are presented. There, sequential 2D images show the collagen arrangement at different depths, indicating a variation of the fiber orientation throughout mural thickness. The fiber orientation shows an increasing deviation from the circumferential direction with increasing depth of the measurements in radial direction, which aligns with the numerical results obtained in the presented numerical examples. A morphological analysis of non-atherosclerotic tissue samples from human abdominal aortas is presented in Schriefl et al. [2012] and also displays a change of the collagen orientation throughout mural thickness, including data for the media as well as the adventitia layer of the artery. The measurements also show an increasing fiber angle from the circumferential to the axial direction over the thickness of the tissue sample. Nevertheless, O'Connell et al. [2008] and Schriefl et al. [2012] indicate that the media is rather composed of a stack of thin layers with one preferred fiber directions in each of the layers with alternating orientations. These alternating single fiber family layers which are dominant in the media are only phenomenologically governed by the material model used in this contribution, which considers the superposition of two transversely isotropic models. Furthermore, the fiber reorientation leads to a significant drop in the axial Cauchy stresses while the circumferential Cauchy stresses remain almost the same, cf. Figure 7. To compare the computational effort with the original algorithm in Hariton et al. [2007a] we compute the number of required incremental steps. In this example, a number of 10 load steps is required to obtain a converging solution for the full load and thus, multiplying this with the number of 5 reorientation steps yields $n^{\text{total}}_{(\text{HDGH})} = 50$. Inserting this in (4)

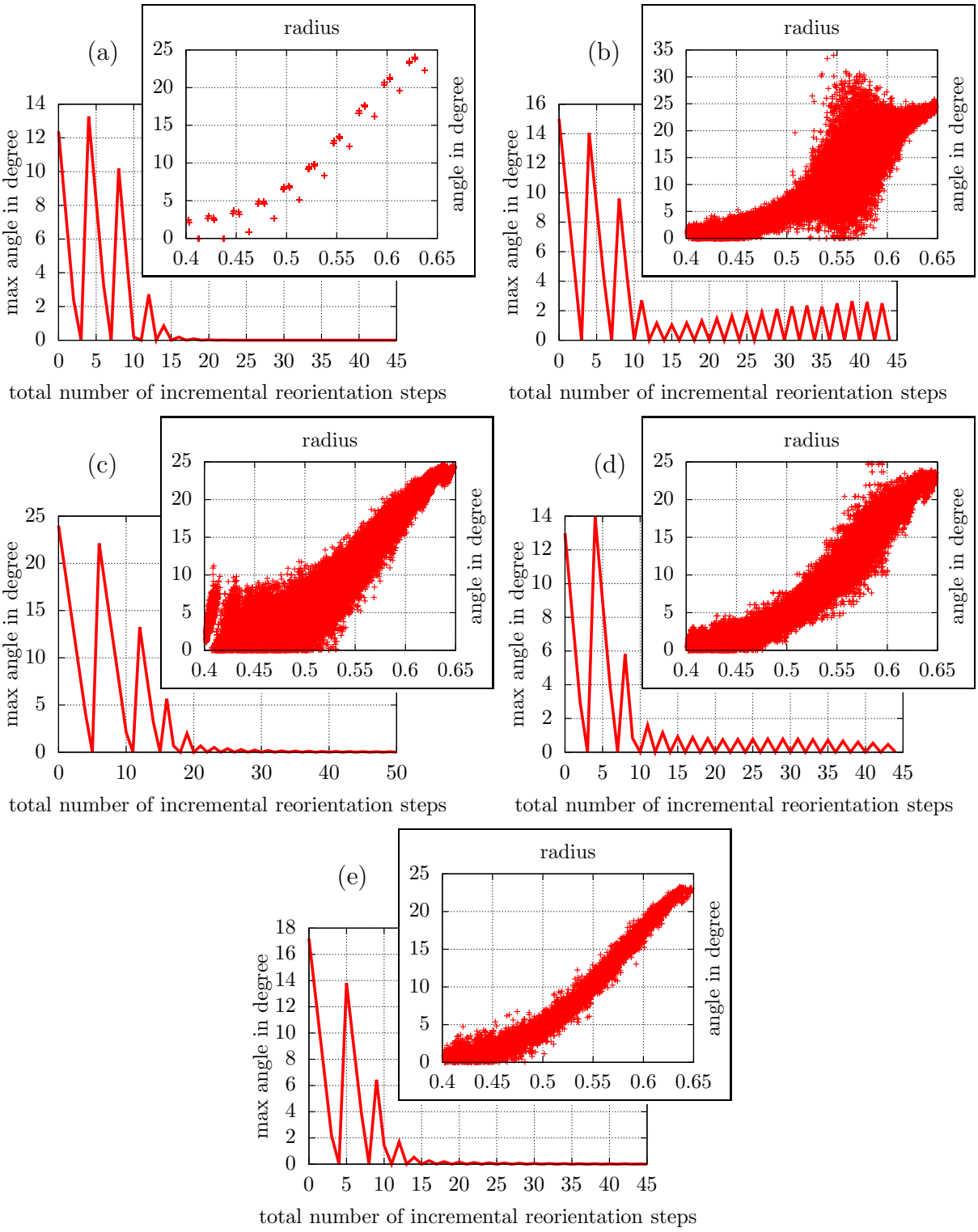

Figure 6: Comparison of the maximum change in the fiber angle within the whole domain in between reorientation steps and the final distribution of the fiber angle over the radius for: (a) Approach σ^l with P_2 brick elements, (b) Approach σ^l with P_2 tetrahedral elements, (c) Approach σ^l with tetrahedral $\bar{F}$-elements, (d) Approach $\bar{\sigma}$ with P_2 tetrahedral elements and (e) Approach $\bar{\sigma}$ with tetrahedral $\bar{F}$-elements. Best performance with view to few noise in the resulting fiber orientation as well as velocity of convergence of the reorientation algorithm is obtained for $\bar{F}$-elements using Approach $\bar{\sigma}$.

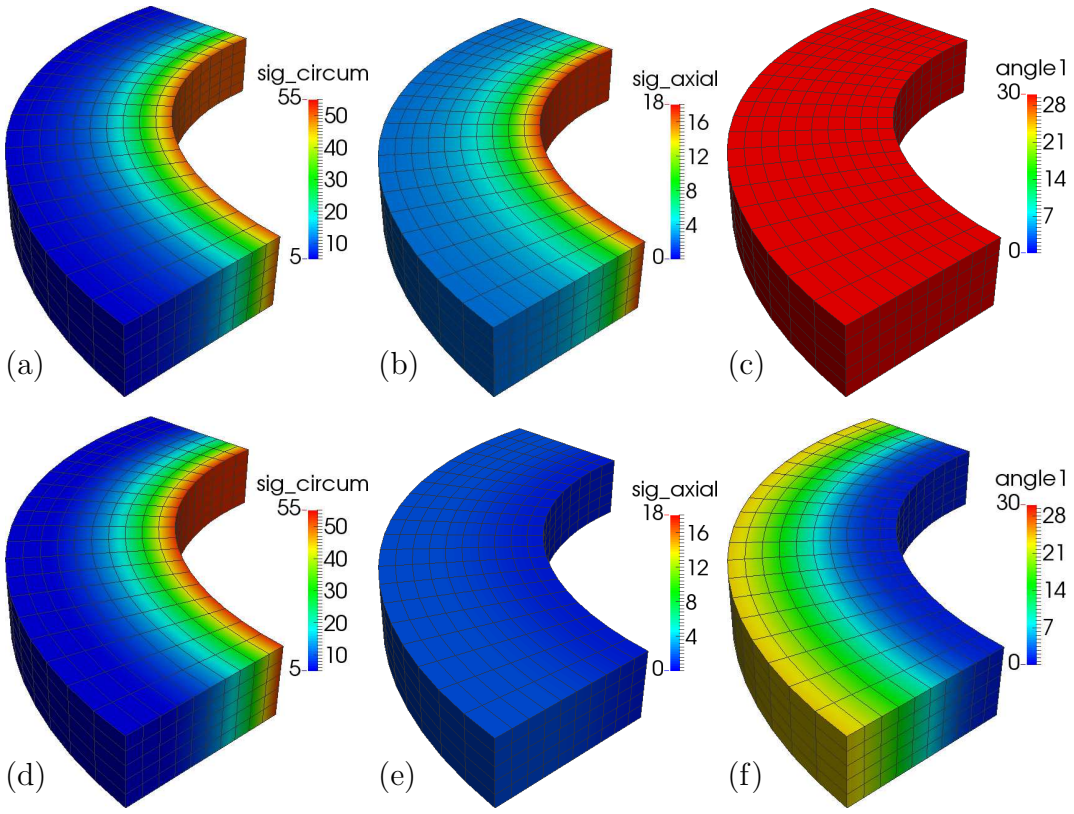

Figure 7: Approach σ^l using brick elements. Before reorientation: (a) circumferential Cauchy stresses, (b) axial Cauchy Stresses and (c) fiber angle. After reorientation: (d) circumferential Cauchy stresses, (e) axial Cauchy Stresses and (f) fiber angle.

yields $f_{\text{comp}} = 0.3$, i.e. the computational effort of the proposed approach is only 30 % of the effort needed using the approach in Hariton et al. [2007a].

Approach σ^l with P_2 tetrahedral elements: In the second example 10 noded tetrahedral elements with quadratic shape functions are used to discretize the geometry. Once again approach σ^l is used for the fiber reorientation, but here the results strongly deviate from the results obtained considering the brick elements. Figure 6(b) shows that no final fiber orientation is obtained throughout the reorientation process, i.e. the maximum change in the fiber angle is increasing towards the end of the computation. Even though the distribution of the fiber angle over the thickness of the artery shows a similar bias as before, the fiber angle is significantly scattered over a wide range especially in the third fourth of the radius. Surprisingly, this observation is not recognizable by simply comparing the contour plots in Figure 7 and Figure 8. The reason for the strong noise in the fiber orientation is most probably the mesh anisotropy induced by the tetrahedral discretization which does not enable element edges following the rotation symmetry. This already leads to not fully rotation-symmetric stress distributions before the reorientation process.

Approach σ^l with tetrahedral $\bar{F}$-elements: Since the standard quadratic tetrahedral elements do not yield the same quality of results as the brick elements, in this example the element formulation is improved by considering a $\bar{\text{F}}$-element formulation, cf. Simo et al. [1985]. Once again the improvement is not recognizable by only considering the contour plots of the stress and fiber angle distribution since they are very similar to the ones in Figure 8. Nevertheless, the maximum change of fiber orientation between the reorientation steps shows a significantly improved convergence behavior by reaching a final fiber

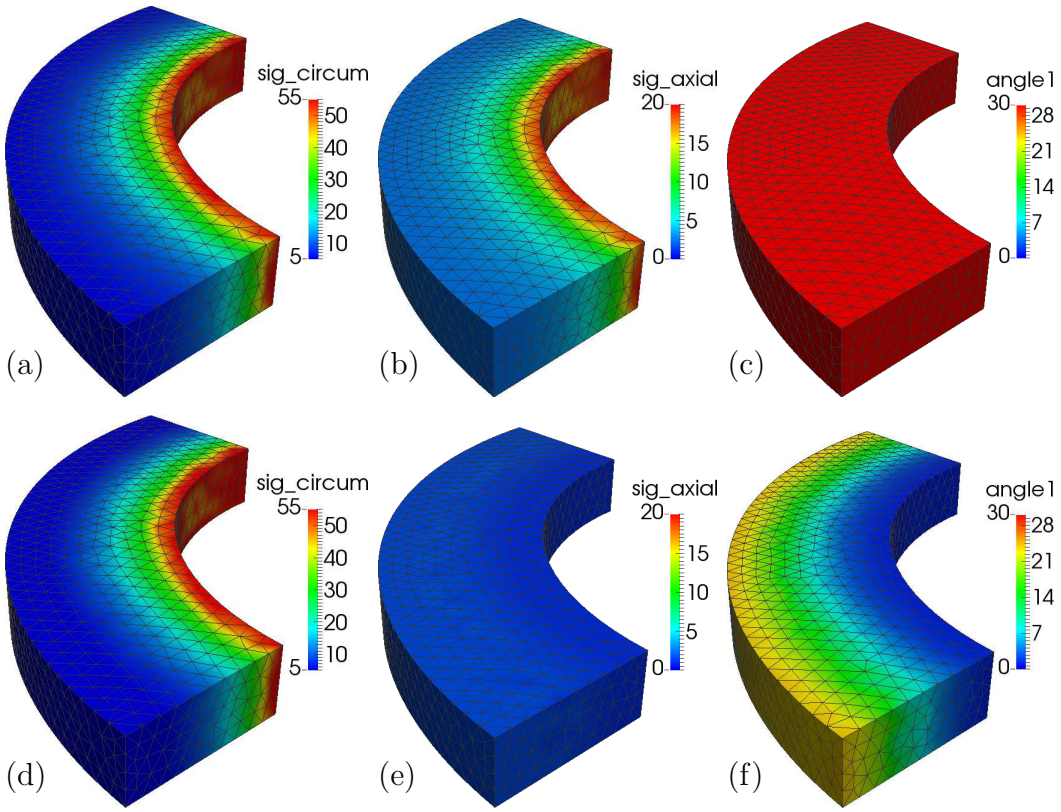

Figure 8: Approach σ^l using tetrahedral elements. Before reorientation: (a) Circumferential Cauchy stresses, (b) Axial Cauchy Stresses and (c) Fiber angle. After reorientation: (d) Circumferential Cauchy stresses, (e) Axial Cauchy Stresses and (f) Fiber angle.

orientation in 20 incremental reorientation steps, i.e. 5 reorientation steps and 67 Newton iterations. The distribution of the fiber angle, however, still shows large fluctuations over the radius, especially in the range of smaller fiber angles, cf. Figure 6(c).

Approach $\bar{\sigma}$ with P_2 tetrahedral elements: In order to improve the results, besides improving the element formulation, we directly access the reorientation model. Therefore, here the extended model $\bar{\sigma}$, based on volume-averaged principal stresses, is used. Thereby, the influence of a Gauss-Point-wise scattering of the stresses onto the reorientation procedure is relaxed and the final fiber orientation is obtained after 16 incremental reorientation steps, i.e. 6 reorientation steps and 50 Newton iterations, see Figure 6(d). Actually, the biggest improvement is found in the fiber angle distribution throughout mural thickness, since less noise and more regularity in the distribution of the fiber angle are obtained.

Approach $\bar{\sigma}$ with tetrahedral $\bar{F}$-elements: Now a combination of the $\bar{\mathrm{F}}$ elements and the average model $\bar{\sigma}$ is used. The results show a good convergence behavior in the sense of the maximum change in the fiber angle as well as for the distribution of the fiber angle over the thickness of the artery, see Figure 6(e). In detail the final fiber orientation is obtained after $n^{\text{total}}_{(\text{FBS})} = 15$ incremental reorientation steps, i.e. 4 reorientation steps and 46 Newton iterations. In comparison this approach combines a strong convergence behavior with a reasonable fiber distribution, even though small fluctuations in the fiber angle distribution remain. However, it may be a suitable method for more complex-shaped arteries as patient-specific ones, because the good geometric approximation performance of tetrahedral elements can be combined with few numerical scattering of the fiber orientation and good reorientation convergence behavior.

5.3. Patient-Specific Artery

In this section the most successful approach, i.e. the $\bar{\mathrm{F}}$-element formulation in combination with approach $\bar{\sigma}$, is applied to the inflation of a patient-specific geometric model of an artery. Therefore, we focus on the Virtual Histology method which provides information regarding a stack of axially distributed two-dimensional cross-section images from which the morphology as well as the individual components of the arterial wall such as the media, adventitia and plaque can be segmented, for further information please be referred to Balzani et al. [2012]. Here, a short segment from a human coronary artery is considered. The actual components like adventitia, media and plaque are replaced by a single material representing the media for this BVP. Similar to the idealized arterial geometry the top and bottom cross sections are fixed in axial direction. Furthermore, at both cross-sections three nodes are fixed such that the radial inflation is unconstrained, while the system is kept statically determined, cf. Figure 9(a). Then the fiber reorientation is algorithm is applied at an internal pressure of 10 kPa. The initial fiber orientation is set to a fiber angle of $\beta_f = 30°$. The convergence behavior for the patient-specific artery is depicted in Figure 9(a) and shows that a final fiber orientation is obtained after 55 incremental reorientation steps, i.e. 19 reorientation steps and 185 Newton iterations. The first and second principal Cauchy stresses are depicted in Figure 10. While the first principal stress σ_I is barely influenced, σ_{II} shows a clear reduction throughout the reorientation process. Figure 9(b) shows the "circumferential" fiber alignment (with almost no "radial" component of fiber orientation) for the updated fiber configuration. The pitch of the fibers in "axial" direction are depicted in Figure 10(c) and (f) with respect to the fiber angle β_{f}. The fiber angle is ranging between 0° and 45° and increasing over the thickness of the artery and additionally seems to be influenced by the fluctuating thickness of the artery. Here, the required number of load steps is again 10 and thus, the total number of incremental load steps for the approach in Hariton et al. [2007a] would be $n^{\mathrm{total}}_{(\mathrm{HDGH})} = 19 \times 10 = 190$. Our approach requires a total number of incremental reorientation steps $n^{\mathrm{total}}_{(\mathrm{FBS})} = 55$ and thus, the efficiency factor is $f_{\mathrm{comp}} = 0.29$. Note, that although we consider an outer geometry of the artery which is patient-specific, the composition is rather simple since only one material is taken into account. In a real artery, separate layers with strongly differing material coefficients would occur and significantly increase the required number of incremental load steps. Another example for a more complex numerical problem would e.g. be to incorporate the fluid-structure interaction. The number of load steps may then increase to e.g. 100, 1000 or even more. This will result in a dramatic further efficiency gain of the proposed method, i.e. the efficiency factors would be $f_{\mathrm{comp}} = 0.029$, $f_{\mathrm{comp}} = 0.0029$ or even less. Thereby, a significant reduction in computational effort could be realized by the proposed method.

5.4. Consideration of Residual Stresses

Here we evaluate the effects of residual stresses in combination with the fiber reorientation update scheme proposed in this paper. The modus operandi is based on the novel approach for the calculation of residual stresses proposed in Schröder and von Hoegen [2015], see also Schröder and Brinkhues [2014]. In this approach the circumferential stresses are smoothened over the thickness of the artery by incorporating residual stresses which are defined as the difference of the stresses in circumferential direction and their volume av-

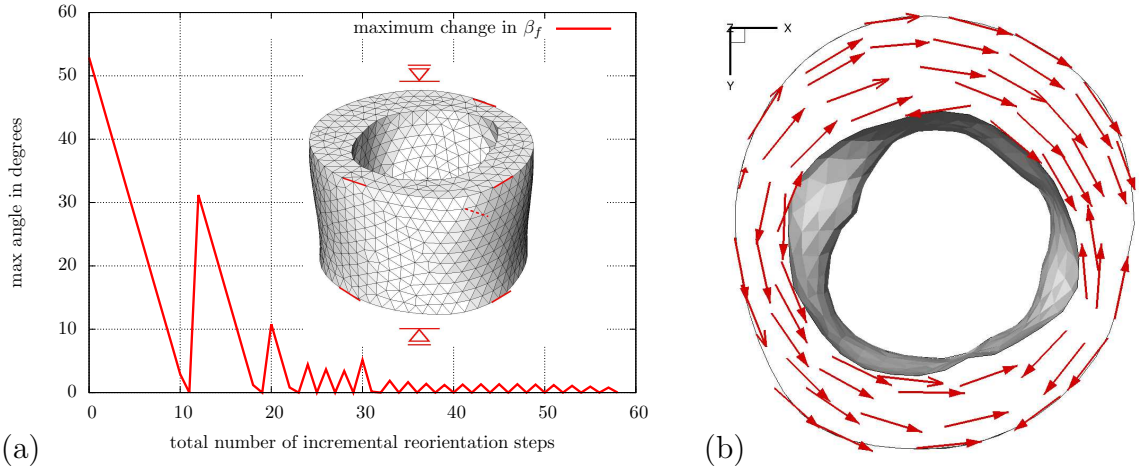

Figure 9: Patient-specific artery: (a) maximum change in the fiber angle within the whole domain between reorientation steps. (b) top view of the fiber orientation of $\boldsymbol{A}_{(1)}$ after fiber reorientation.

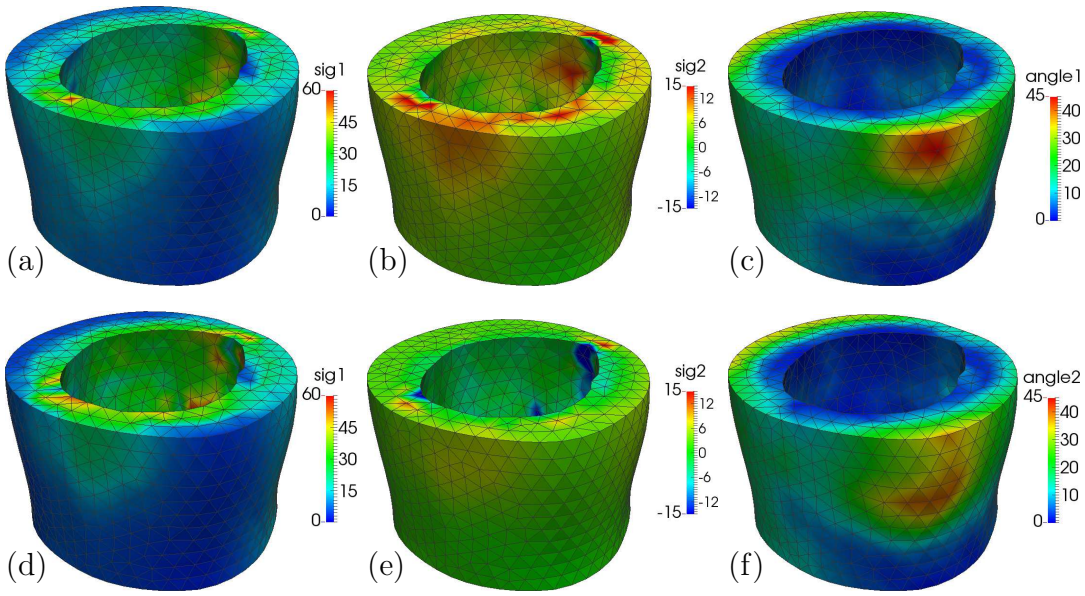

Figure 10: Patient-specific artery. Before reorientation: (a) σ_I, (b) σ_{II}. After reorientation: (c) fiber angle of fiber family $\boldsymbol{A}_{(1)}$, (d) σ_I, (e) σ_{II} and (f) fiber angle of fiber family $\boldsymbol{A}_{(2)}$.

erage computed over predefined segments. In order to obtain a smooth stress distribution these residual stresses are applied and recalculated in several smoothing loops. The procedure is as follows: First, an internal pressure, corresponding to a reasonable blood pressure of 80 mmHg is applied. In a second step an additional axial pre-stress, corresponding to an axial stretch of 5% acting on the already deformed geometry, is applied. This is in line with the axial pre-stretch found in arteries. Then the reorientation algorithm is carried out until a converged field of fiber direction vectors is obtained. At last, the residual stresses are applied. For our analysis we again consider the idealized artery geometry from Section 5.2. The adapted fiber orientation as well as the convergence behavior of the reorientation algorithm are strongly influenced by the axial boundary conditions. Figure 11 shows an increased fiber angle gradient over the thickness of the arterial wall in case of the pre-stress. In detail, the fiber angle ranges between 13° and 54° with respect to the

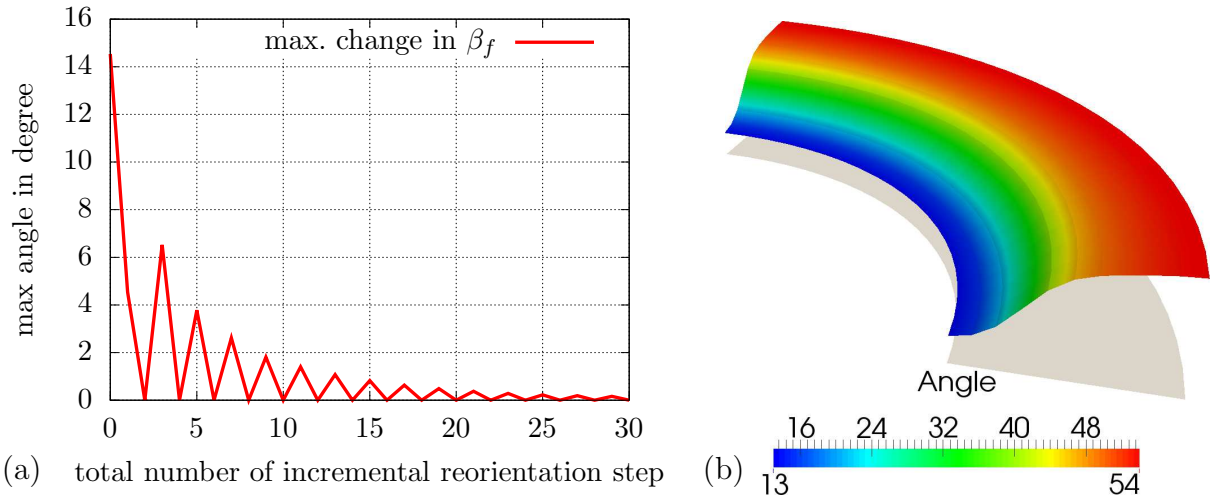

Figure 11: Application of reorientation as well as residual stress approach: (a) Maximum change in the fiber angle within the whole domain in between reorientation steps. (b) Fiber angle distribution over the radius.

circumferential plane, with a steep incline of the fiber angle distribution at the inner side of the arterial wall and an almost constant fiber angle at the outer half of the rotationally symmetric geometry. In Figure 12 results for the idealized arterial segments are shown. Here, different stress quantities, i.e. stresses in circumferential direction, axial direction and residual stresses in circumferential direction, as well as the fiber angle distribution, are compared. Furthermore, four different stages of the computation are examined: (a) application of the stress boundary conditions (blood pressure and axial pre-stress), (b) changes due to the fiber reorientation algorithm, (c) the residual stresses in circumferential direction and (d) the combination of the fiber reorientation algorithm and the residual stresses in circumferential direction. It turns out that the fiber reorientation algorithm appears to decrease the gradient of the axial stresses, while the residual stress approach decreases the gradient of the circumferential stresses, as expected. The superposition of both approaches leads to a decrease of both stress gradients, even though this causes an increase of the circumferential residual stresses and a slight increase of the axial stress gradient. Note that both phenomena, fiber reorientation and residual stresses will take place simultaneously in arterial walls. Hence, a nested algorithm iterating between both approaches might be more suitable to consider the effects of fiber reorientation and residual stresses at the same time. First steps towards a nested algorithm have been considered but, admittedly, did not yield promising results yet.

Remarks on a Nested Approach for Residual Stresses and Fiber Reorientation: Here, a nested algorithm iterating between the residual stress approach and the fiber orientation approach is presented. Even though, this algorithm does not yield promising results yet, its results are presented and discussed critically in this context. First of all a reasonable initial configuration for the fiber angle is determined, following the boundary value problem from Section 5.2, cf. Figure 12 row (a). In a next step the residual stresses are applied, taking into account several smoothing loops until an almost homogenous circumferential stress distribution is obtained. From here, the fiber angle is adjusted incrementally in 10° steps, where each step is followed by several residual stress smoothing loops. This procedure is then repeated ten times. The convergence behavior of the fiber angle as well as the fiber angle distribution in the last iteration step are depicted in Figure 13. While a good

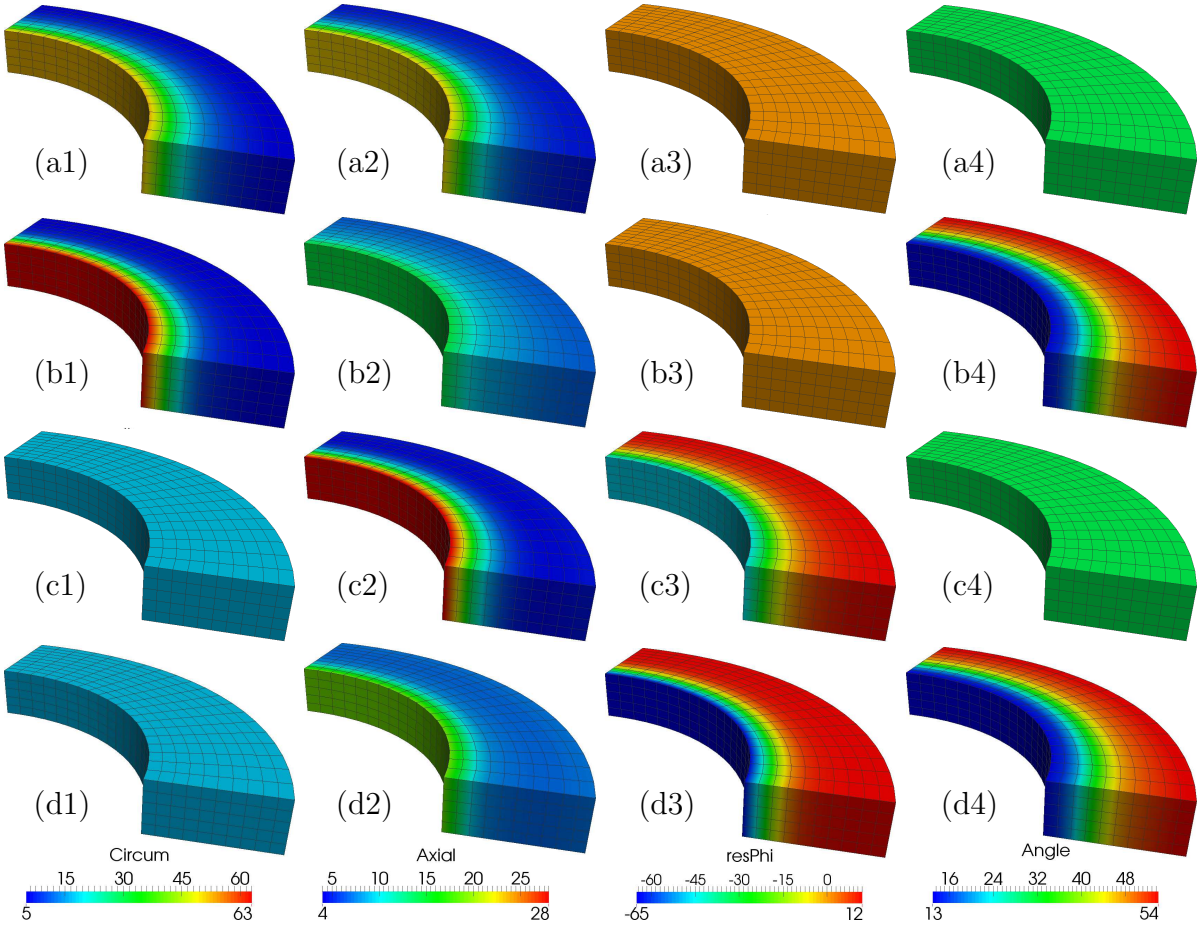

Figure 12: Comparison residual stresses/fiber reorientation including axial pre-stress; Columns: (1) circumferential stresses, (2) axial stresses, (3) residual stresses in circumferential direction and (4) fiber angle distribution over the radius. Rows: (a) application of stress boundary conditions (blood pressure and axial pre-stress), (b) fiber reorientation algorithm, (c) residual stresses, (d) combined approach.

convergence behavior for the initial configuration is obtained, cf. Figure 13(a) reorientation steps 1-20, the nested iteration which is repeated ten times, does not show any convergence but is rather switching back and forth between 28° and 18° for the remaining change of the fiber angle, cf. Figure 13(a) reorientation steps 20-30. The resulting fiber angle distribution shows a steep gradient at the inside of the geometry, followed by solely circumferentially oriented fibers in the middle and a slight incline towards the outside of the geometry which may be considered as unphysiological.

6. Conclusion

An algorithmic scheme for the calculation of fiber orientations in arterial walls based on the direction and magnitude of principal stresses is proposed. The approach extends the procedure proposed in Hariton et al. [2007a] to enable a higher computational efficiency. In addition to that, a modified model for the favored fiber orientation was proposed in terms of volume-averages of stresses computed over individual finite elements, which stabilizes the convergence behavior of the reorientation procedure. Several numerical studies

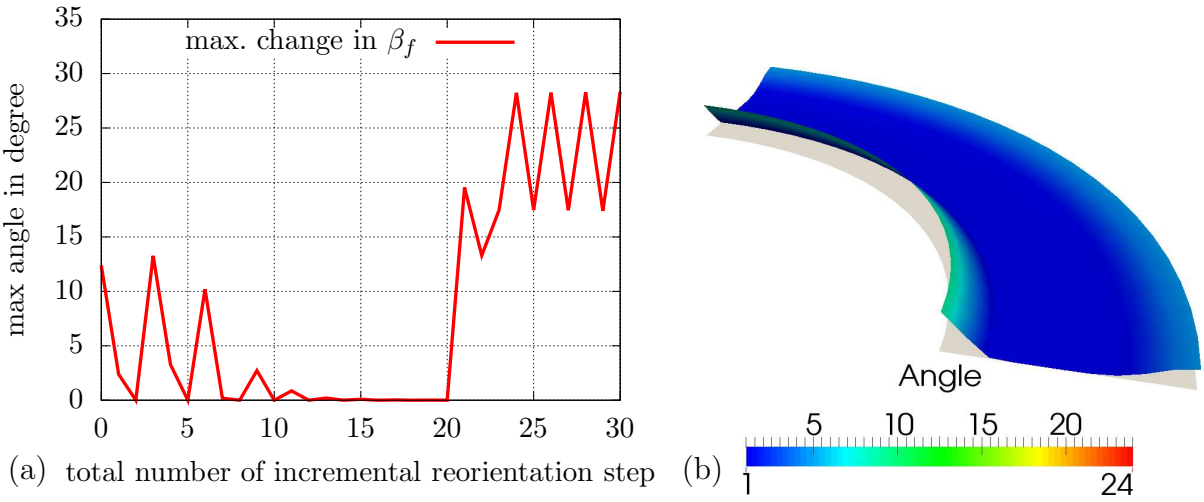

Figure 13: Nested application of reorientation and residual stress approach: (a) Maximum change in the fiber angle within the whole domain in between reorientation steps. (b) Unphysiological fiber angle distribution over the radius.

were performed to analyze the performance of the proposed approaches. The stress-driven model for the favored fiber orientation from Hariton et al. [2007a] was compared with the one from Cyron and Humphrey [2014] in a simple biaxial tension test. It was found that the total strain energy in the test specimen could be decreased by the fiber reorientation scheme. However, a more pronounced reduction was observed for the approach proposed in Hariton et al. [2007a], which is also considered here. Inhomogeneous boundary value problems were also taken into account, where an inflated idealized arterial wall was considered. Different finite element formulations and two different models for the favored fiber orientation were compared in order to analyze the influence of the stress approximation accuracy on the reorientation algorithm. It was found that in particular for tetrahedral elements a significant improvement could be obtained by using a mixed $\bar{F}$-element formulation and the extended model based on the volume averages of principal stresses. There, a stabilized convergence of the reorientation scheme and less noise in the resulting fiber orientation was observed. This improved approach has been applied to a patient specific geometric model of an atherosclerotic artery, where a converged fiber orientation could be obtained. For these two numerical examples the advantage of the proposed algorithmic scheme was evaluated and a speed-up of more than 300 % could be realized. It turned out that for more complex boundary value problems this speed-up can easily increase up to 3000 % or higher. Finally, the algorithm for the fiber reorientation was combined with an approach for circumferential residual stresses and the effects of both phenomena were examined. The superposition of both approaches results in a smoothing of the circumferential and a reduction in axial stress distributions. On the other hand a nested approach did not directly yield physiological results and will be part of further examinations. Furthermore, the influence of fluid-structure-interaction on the orientation of collagen fibers and vice versa will be examined in the future, taking into account the fluid-structure-interaction framework presented in Balzani et al. [2015].

7. Acknowledgment

Financial support of the German Science Foundation (DFG) under the project no. SCHR570/15-1 and BA2823/9-1 is highly acknowledged. The author D. Balzani additionally thanks the DFG for funding in the context of the Institutional Strategy "The Synergetic University" at TU Dresden, as part of the Excellence Initiative. Furthermore the cooperation with our co-worker Markus von Hoegen, especially in the context of residual stresses in arterial walls, is highly acknowledged.

References

J.M. Ball. Convexity conditions and existence theorems in non-linear elasticity. Archive of Rational Mechanics and Analysis, 63:337–403, 1977.

D. Balzani, P. Neff, J. Schröder, and G.A. Holzapfel. A polyconvex framework for soft biological tissues. adjustment to experimental data. International Journal of Solids and Structures, 43(20):6052–6070, 2006.

D. Balzani, D. Böse, D. Brands, R. Erbel, A. Klawonn, O. Rheinbach, and J. Schröder. Parallel simulation of patient-specific atherosclerotic arteries for the enhancement of intravascular ultrasound diagnostics. Engineering Computations, 29(8), 2012.

D. Balzani, S. Deparis, S. Fausten, D. Forti, A. Heinlein, A. Klawonn, A. Quarteroni, O. Rheinbach, and J. Schröder. Numerical modeling of fluid-structure interaction in arteries with anisotropic polyconvex hyperelastic and anisotropic viscoelastic material models at finite strains. International Journal for Numerical Methods in Biomedical Engineering, 2015. ISSN 2040-7947. doi: 10.1002/cnm.2756. URL `http://dx.doi.org/10.1002/cnm.2756`.

J.P. Boehler. Introduction to the invariant formulation of anisotropic constitutive equations. In J.P. Boehler, editor, Applications of Tensor Functions in Solid Mechanics, number 292 in Courses and Lectures of CISM, pages 13–30. Springer, 1987.

D. Brands, A. Klawonn, O. Rheinbach, and J. Schröder. Modelling and convergence in arterial wall simulations using a parallel FETI solution strategy. Computer Methods in Biomechanics and Biomedical Engineering, 11(5):569–583, 2008.

A. Creane, E. Maher, S. Sultan, N. Hynes, D.J. Kelly, and C. Lally. Prediction of fibre architecture and adaptation in diseased carotid bifurcations. Biomechanics and Modeling in Mechanobiology, 10:831–843, 2011.

A. Creane, E. Maher, S. Sultan, N. Hynes, D.J. Kelly, and C. Lally. A remodelling metric for angular fibre distributions and its application to diseased carotid bifurcations. Biomechanics and Modeling in Mechanobiology, 11:869–882, 2012.

C.J. Cyron and J.D. Humphrey. Preferred fiber orientations in healthy arteries and veins understood from netting analysis. Mathematics and Mechanics of Solids, pages 1–17, 2014.

N. Driessen, W. Wilson, C. Bouten, and F. Baaijens. A computational model for collagen fibre remodelling in the arterial wall. Journal of Theoretical Biology, 226(1):53–64, 2004.

N. Driessen, G. Peters, J. Huyghe, C. Bouten, and F. Baaijens. Remodelling of continuously distributed collagen fibres in soft connective tissues. Journal of Biomechanics, 36 (8):1151–1158, 2008.

A. Grillo, G. Wittum, and S. Tomic, A. Federico. Remodelling in statistically oriented fibre-reinforced materials and biological tissues. Mathematics and Mechanics of Solids, 20:1107–1129, 2015.

I. Hariton, G. deBotton, T.C. Gasser, and G.A. Holzapfel. Stress-driven collagen fiber remodeling in arterial walls. Biomechanics and Modeling in Mechanobiology, 6(3): 163–175, 2007a.

I. Hariton, G. deBotton, T.C. Gasser, and G.A. Holzapfel. Stress-modulated collagen fiber remodeling in a human carotid bifurcation. Journal of Theoretical Biology, 248 (3):460–470, 2007b.

S. Hartmann and P. Neff. Polyconvexity of generalized polynomial-type hyperelastic strain energy functions for near-incompressibility. International Journal of Solids and Structures, 40:2767–2791, 2003.

G. Himpel, A. Menzel, E. Kuhl, and P. Steinmann. Time-dependent fibre reorientation of transversely isotropic continua-finite element formulation and consistent linearization. International Journal for Numerical Methods in Engineering, 73(10):1413–1433, 2008.

G. Holzapfel. Determination of material models for arterial walls from uniaxial extension tests and histological structure. Journal of Theoretical Biology, 238(2):290–302, 2006.

G.A. Holzapfel, T.C. Gasser, and R.W. Ogden. A new constitutive framework for arterial wall mechanics and a comparative study of material models. Journal of Elasticity and the Physical Science of Solids, 61(1-3):1–48, 2000.

E. Kuhl and G.A. Holzapfel. A continuum model for remodeling in living structures. Journal of Materials Science, 42(21):8811–8823, 2007.

A. Menzel and T. Waffenschmidt. A microsphere-based remodelling formulation for anisotropic biological tissues. Philosophical Transactions of the Royal Society A, 367: 3499–3523, 2009.

M.K. O'Connell, S. Murthy, S. Phan, C. Xu, J. Buchanan, R. Spilker, R.L. Dalman, C.K. Zarins, W. Denk, and C.A. Taylor. The three-dimensional micro- and nanostructure of the aortic medial lamellar unit measured using 3d confocal and electron microscopy imaging. Matrix Biology, 27:171–181, 2008.

N. Qi, R.W. Ogden, N.A. Hill, G.A. Holzapfel, H. Han, and X. Luo. Investigation of the optimal collagen fibre orientation in human iliac arteries. Journal of the Mechanical Behavior of Biomedical Materials, 61, 2015. doi: http://dx.doi.org/10.1016/j.jmbbm.2015.06.11.

C. Sansour. On the physical assumptions underlying the volumetric-isochoric split and the case of anisotropy. European Journal of Mechanics - A/Solids, 27:28–39, 2008.

A.J. Schriefl, H. Wolinski, P. Regitnig, S.D. Kohlwein, and G.A. Holzapfel. An automated approach for three-dimensional quantification of fibrillar structures in optically cleared soft biological tissues. Journal of the Royal Society Interface, 10(80), 2012. doi: 10.1098/rsif.2012.0760. URL `http://rsif.royalsocietypublishing.org/content/10/80/20120760`.

J. Schröder. Anisotropic polyconvex energies. In Poly-, Quasi- and Rank-One Convexity in Applied Mechanics, volume 516, pages 53–105. Springer-Verlag, 2010.

J. Schröder and S. Brinkhues. A novel scheme for the approximation of residual stresses in arterial walls. Archive of Applied Mechanics, 84:881–898, 2014.

J. Schröder and P. Neff. Invariant formulation of hyperelastic transverse isotropy based on polyconvex free energy functions. International Journal of Solids and Structures, 40: 401–445, 2003.

J. Schröder and M. von Hoegen. An engineering tool to estimate eigenstresses in three-dimensional patient-specific arteries. Computer Methods in Applied Mechanics and Engineering, under review, 2015.

J. Schröder, P. Neff, and D. Balzani. A variational approach for materially stable anisotropic hyperelasticity. International Journal of Solids and Structures, 42(15):4352–4371, 2005.

J.C. Simo, R.L. Taylor, and K.S. Pister. Variational and projection methods for the volume constraint in finite deformation elasto-plasticity. Computer Methods in Applied Mechanics and Engineering, 51:177–208, 1985.

R.L. Taylor. FEAP - finite element analysis program, 2014. URL `http://www.ce.berkeley/feap`.

T. Waffenschmidt and A. Menzel. Extremal states of energy of a double-layered thick-walled tube - application to residually stressed arteries. Journal of the Mechanical Behavior of Biomedical Materials, 29:635–654, 2014. doi: http://dx.doi.org/10.1016/j.jmbbm.2013.05.023.